IMPLICIT CAUSAL MODELS FOR GENOME-WIDE ASSOCIATION STUDIES

Anonymous authors
Paper under double-blind review

ABSTRACT

Progress in probabilistic generative models has accelerated, developing richer models with neural architectures, implicit densities, and with scalable algorithms for their Bayesian inference. However, there has been limited progress in models that capture causal relationships, for example, how individual genetic factors cause major human diseases. In this work, we focus on two challenges in particular: How do we build richer causal models, which can capture highly nonlinear relationships and interactions between multiple causes? How do we adjust for latent confounders, which are variables influencing both cause and effect and which prevent learning of causal relationships? To address these challenges, we synthesize ideas from causality and modern probabilistic modeling. For the first, we describe *implicit causal models*, a class of causal models that leverages neural architectures with an implicit density. For the second, we describe an implicit causal model that adjusts for confounders by sharing strength across examples. In experiments, we scale Bayesian inference on up to a billion genetic measurements. We achieve state of the art accuracy for identifying causal factors: we significantly outperform the second best result by an absolute difference of 15-45.3%.

1 INTRODUCTION

Probabilistic models provide a language for specifying rich and flexible generative processes (Pearl, 1988; Murphy, 2012). Recent advances expand this language with neural architectures, implicit densities, and with scalable algorithms for their Bayesian inference (Rezende et al., 2014; Tran et al., 2017). However, there has been limited progress in models that capture high-dimensional causal relationships (Pearl, 2000; Spirtes et al., 1993; Imbens & Rubin, 2015). Unlike models which learn statistical relationships, causal models let us manipulate the generative process and make counterfactual statements, that is, what would have happened if the distributions changed.

As the running example in this work, consider genome-wide association studies (GWAS) (Yu et al., 2005; Price et al., 2006; Kang et al., 2010). The goal of GWAS is to understand how genetic factors, i.e., single nucleotide polymorphisms (SNPs), cause traits to appear in individuals. Understanding this causation both lets us predict whether an individual has a genetic predisposition to a disease and also understand how to cure the disease by targeting the individual SNPs that cause it.

With this example in mind, we focus on two challenges to combining modern probabilistic models and causality. The first is to develop richer, more expressive causal models. Probabilistic causal models represent variables as deterministic functions of noise and other variables, and existing work usually focuses on additive noise models (Hoyer et al., 2009) such as linear mixed models (Kang et al., 2010). These models apply simple nonlinearities such as polynomials, hand-engineered low order interactions between inputs, and assume additive interaction with Gaussian noise. In GWAS, strong evidence suggests that susceptibility to common diseases is influenced by epistasis (the interaction between multiple genes) (Culverhouse et al., 2002; McKinney et al., 2006). We would like to capture and discover such interactions. This requires models with nonlinear, learnable interactions among the inputs and the noise.

The second challenge is how to address latent population-based confounders. In GWAS, both latent population structure, i.e., subgroups in the population with ancestry differences, and relatedness among sample individuals produce spurious correlations among SNPs to the trait of interest. Existing methods correct for this correlation in two stages (Yu et al., 2005; Price et al., 2006; Kang et al.,

2010): first, estimate the confounder given data; then, run standard causal inferences given the estimated confounder. These methods are effective in some settings, but they are difficult to understand as principled causal models, and they cannot easily accommodate complex latent structure.

To address these challenges, we synthesize ideas from causality and modern probabilistic modeling. For the first challenge, we develop *implicit causal models*, a class of causal models that leverages neural architectures with an implicit density. With GWAS, implicit causal models generalize previous methods to capture important nonlinearities, such as gene-gene interaction, when modeling the trait of interest. Building on this, for the second challenge, we describe an implicit causal model that adjusts for population-confounders by sharing strength across examples. We lay out conditions that prove the model consistently estimates the causal relationship. This model both justifies existing methods and extends them to more complex latent variable models of the confounder.

In experiments, we scale Bayesian inference on implicit causal models on up to a billion genetic measurements. Validating these results are not possible for observational data (Pearl, 2000), so we first perform an extensive simulation study of 11 configurations of 100,000 SNPs and 940 to 5,000 individuals. We achieve state of the art accuracy for identifying causal factors: we significantly outperform the second best result by an absolute difference of 15-45.3%. In a real-world GWAS, we also show our model discovers real causal relationships—identifying similar SNPs as previous state of the art—while being more principled as a causal model.

1.1 Related work

There has been growing work on richer causal models. Louizos et al. (2017) develop variational auto-encoders for causality and address local confounders via proxy variables. Our work is complementary: we develop implicit models for causality and address global confounders by sharing strength across examples. In other work, Mooij et al. (2010) propose a Gaussian process over causal mechanisms, and Zhang & Hyvärinen (2009) study post-nonlinear models, which apply a nonlinearity after adding noise. These models typically focus on the task of causal discovery, and they assume fixed nonlinearities or smoothness which we relax using neural networks. In the potential outcomes literature, much recent work has considered decision trees and neural networks (e.g., Hill (2011); Wager & Athey (2015); Johansson et al. (2016)). These methods tackle a related but different problem of balancing covariates across treatments.

Causality with population-confounders has primarily been studied for genome-wide association studies (GWAS). A popular approach is to first, estimate the confounder using the top principal components of the genotype matrix of individuals-by-SNPs; then, linearly regress the trait of interest onto the genetic factors and these components (Price et al., 2006; Astle & Balding, 2009). Another approach is to first, estimate the confounder via a "kinship matrix" on the genotypes; then, fit a linear mixed model of the trait given genetic factors, and where the covariance of random effects is the kinship matrix (Yu et al., 2005; Kang et al., 2010). Other work adjusts for the confounder via admixture models and factor analysis (Song et al., 2015; Hao et al., 2016). This paper builds on all these methods, providing a theoretical understanding about when causal inferences can succeed while adjusting for latent confounders. We also develop a new causal model with nonlinear, learnable gene-gene and gene-population interactions; and we describe a Bayesian inference algorithm that justifies the two-stage estimation.

The problem of epistasis, that is, nonadditive interactions between multiple genes, dates back to classical work on epigenetics by Bateson and R.A. Fisher (Fisher, 1918). Primary methods for capturing epistasis include adding interactions within a linear model, permutation tests, exhaustive search, and multifactor dimensionality reduction (Cordell, 2009). These methods require hand-engineering over all possible interactions, which grows exponentially in the number of genetic factors. Neural networks have been applied to address epistasis for epigenomic data, such as to predict sequence specificities of protein bindings given DNA sequences (Alipanahi et al., 2015). These methods use discriminative neural networks (unlike neural networks within a generative model), and they focus on prediction rather than causality.

2 Implicit Causal Models

We describe the framework of probabilistic causal models. We then describe implicit causal models, an extension of implicit models for encoding complex, nonlinear causal relationships.

Figure 1: Probabilistic causal model. **(left)** Variable x causes y coupled with a shared variable β. **(right)** A more explicit diagram where variables (denoted with a square) are a deterministic function of other variables and noise ϵ (denoted with a triangle).

2.1 Probabilistic Causal Models

Probabilistic causal models (Pearl, 2000), or structural equation models, represent variables as deterministic functions of noise and other variables. As illustration, consider the causal diagram in Figure 1. It represents a causal model where there is a global variable

$$\beta = f_\beta(\epsilon_\beta), \qquad \epsilon_\beta \sim s(\cdot),$$

and for each data point $n = 1, \ldots, N$,

$$\begin{aligned} x_n &= f_x(\epsilon_{x,n}, \beta), & \epsilon_{x,n} &\sim s(\cdot) \\ y_n &= f_y(\epsilon_{y,n}, x_n, \beta), & \epsilon_{y,n} &\sim s(\cdot). \end{aligned} \tag{1}$$

The noise ϵ are background variables, representing unknown external quantities which are jointly independent. Each variable β, x, y is a function of other variables and its background variable.

We are interested in estimating the causal mechanism f_y. It lets us calculate quantities such as the causal effect $p(y \mid \text{do}(X = x), \beta)$, the probability of an outcome y given that we force X to a specific value x and under fixed global structure β. This quantity differs from the conditional $p(y \mid x, \beta)$. The conditional takes the model and filters to the subpopulation where $X = x$; in general, the processes which set X to that value may also have influenced Y. Thus the conditional is not the same as if we had manipulated X directly (Pearl, 2000).

Under the causal graph of Figure 1, the adjustment formula says that $p(y \mid \text{do}(x), \beta) = p(y \mid x, \beta)$. This means we can estimate f_y from observational data $\{(x_n, y_n)\}$, assuming we observe the global structure β. For example, an additive noise model (Hoyer et al., 2009) posits

$$y_n = f(x_n, \beta \mid \theta) + \epsilon_n, \qquad \epsilon \sim s(\cdot),$$

where $f(\cdot)$ might be a linear function of the concatenated inputs, $f(\cdot) = [x_n, \beta]^\top \theta$, or it might use spline functions for nonlinearities. If $s(\cdot)$ is standard normal, the induced density for y is normal with unit variance. Placing a prior over parameters $p(\theta)$, Bayesian inference yields

$$p(\theta \mid \mathbf{x}, \mathbf{y}, \beta) \propto p(\theta) p(\mathbf{y} \mid \mathbf{x}, \theta, \beta). \tag{2}$$

The right hand side is a joint density whose individual components can be calculated. We can use standard algorithms, such as variational inference or MCMC (Murphy, 2012).

A limitation in additive noise models that they typically apply simple nonlinearities such as polynomials, hand-engineered low-order interactions between inputs, and assume additive interaction with Gaussian noise. Next we describe how to build richer causal models. (An additional problem is that we typically don't observe β; we address this in § 3.)

2.2 Implicit Causal Models

Implicit models capture an unknown distribution by hypothesizing about its generative process (Diggle & Gratton, 1984; Tran et al., 2017). For a distribution $p(x)$ of observations x, recent advances define a function g that takes in noise $\epsilon \sim s(\cdot)$ and outputs x given parameters θ,

$$x = g(\epsilon \mid \theta), \quad \epsilon \sim s(\cdot).$$

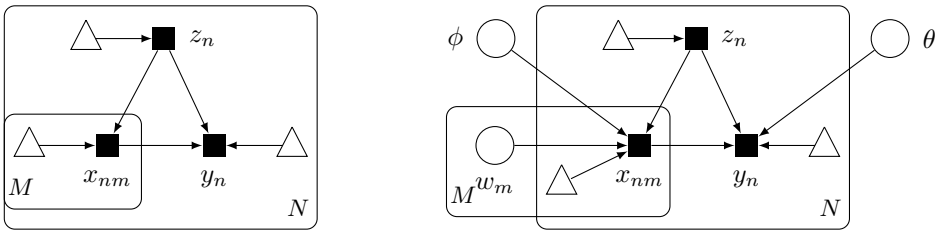

Figure 2: (left) Probabilistic causal model for GWAS. The population structure of SNPs for each individual (z_n) confounds inference of how each SNP (x_{nm}) causes a trait of interest (y_n). **(right)** Implicit causal model for GWAS (described in § 3.2). Its structure is the same as the causal graph but also places priors over parameters ϕ and θ and with a latent variable w_m per SNP.

Unlike models which assume additive noise, setting g to be a neural network enables multilayer, nonlinear interactions. Implicit models also separate randomness from the transformation; this imitates the structural invariance of causal models (Equation 1).

To enforce causality, we define an *implicit causal model* as a probabilistic causal model. Namely, we require that the functions g form structural equations, that is, causal relations among variables. Implicit causal models are nonparametric structural equation models (Pearl, 2000), where the functional forms are themselves learned.

A natural question is the representational capacity of implicit causal models. In general, they are universal approximators: we can use a fully connected network with a sufficiently large number of hidden units to approximate each causal mechanism. We describe this formally.

Theorem (Universal Approximation Theorem)**.** *Let the tuple $(\mathcal{E}, V, F, s(\mathcal{E}))$ denote a probabilistic causal model, where $\mathcal{E}$ represent the set of background variables with probability $s(\mathcal{E})$, V the set of endogenous variables, and F the causal mechanisms. Assume each causal mechanism is a continuous function on the m-dimensional unit cube $f \in \mathcal{C}([0,1]^m)$. Let σ be a nonconstant, bounded, and monotonically-increasing continuous function.*

For each causal mechanism f and any error $\delta > 0$, there exist parameters $\theta = \{\mathbf{v}, \mathbf{w}, \mathbf{b}\}$, for real constants $v_i, b_i \in \mathbb{R}$ and real vectors $w_i \in \mathbb{R}^m$ for $i = 1, \ldots, H$ and fixed H, such that the following function approximates f:

$$g(x \mid \theta) = \sum_{i=1}^{H} v_i \sigma\left(w_i^T x + b_i\right), \qquad |g(x \mid \theta) - f(x)| < \delta \quad \textit{for all } x \in [0,1]^m.$$

The implicit model defined by the collection of functions g and same noise distributions universally approximates the true causal model.

(This directly follows from the approximator theorem of, e.g., Cybenko (1989).) A key aspect is that implicit causal models are not only universal approximators, but that we can use fast algorithms for their Bayesian inference (to calculate Equation 2). In particular, variational methods both scale to massive data and provide accurate posterior approximations (§ 4). This lets us obtain good performance in practice with finite-sized neural networks; § 5 describes such experiments.

3 Implicit Causal Models with Latent Confounders

We described implicit causal models, a rich class of models that can capture arbitrary causal relations. For simplicity, we assumed that we observe the global structure; this enables standard inference methods. We now consider the typical setting when it is unobserved.

3.1 Causal Inference with a Latent Confounder

Consider the running example of genome-wide association studies (GWAS) (Figure 2). There are N data points (individuals). Each data point consists of an input vector of length M (measured SNPs), $x_n = [x_{n1}, \ldots, x_{nM}]$ and a scalar outcome y_n (the trait of interest). Typically, the number of

measured SNPs M ranges from 100,000 to 1 million and the number of individuals N ranges from 500 to 10,000.

We are interested in how changes to each SNP X_m cause changes to the trait Y. Formally, this is the causal effect $p(y \mid \mathrm{do}(x_m), x_{-m})$, which is the probability of an outcome y given that we force SNP $X_m = x_m$ and consider fixed remaining SNPs x_{-m}. Standard inference methods are confounded by the unobserved population structure of SNPs for each individual, as well as the individual's cryptic relatedness to other samples in the data set. This confounder is represented as a latent variable z_n, which influences x_{nm} and y_n for each data index n; see Figure 2. Because we do not observe the z_n's, the causal effect $p(y \mid \mathrm{do}(x_m), x_{-m})$ is unidentifiable (Spirtes et al., 1993).

Building on previous GWAS methods (Price et al., 2006; Yu et al., 2005; Astle & Balding, 2009), we build a model that jointly captures z_n's and the mechanisms for $X_m \to Y$. Consider the implicit causal model where for each data point $n = 1, \ldots, N$ and for each SNP $m = 1, \ldots, M$,

$$\begin{aligned} z_n &= g_z(\epsilon_{z_n}), & \epsilon_{z_n} &\sim s(\cdot), \\ x_{nm} &= g_{x_m}(\epsilon_{x_{nm}}, z_n \mid w_m), & \epsilon_{x_{nm}} &\sim s(\cdot), \\ y_n &= g_y(\epsilon_{y_n}, x_{n,1:M}, z_n \mid \theta), & \epsilon_{y_n} &\sim s(\cdot). \end{aligned} \tag{3}$$

The function $g_z(\cdot)$ for the confounder is fixed. Each function $g_{x_m}(\cdot \mid w_m)$ per SNP depends on the confounder and has parameters w_m. The function $g_y(\cdot \mid \theta)$ for the trait depends on the confounder and all SNPs, and it has parameters θ. We place priors over the parameters $p(w_m)$ and $p(\theta)$.

Figure 2 (left) visualizes the model. It is a model over the full causal graph and differs from the unconfounded case: Equation 2 only requires a model from $X \to Y$, and the rest of the graph is "ignorable" (Imbens & Rubin, 2015).

To estimate the mechanism f_y, we calculate the posterior of the outcome parameters θ,

$$p(\theta \mid \mathbf{x}, \mathbf{y}) = \int p(\mathbf{z} \mid \mathbf{x}, \mathbf{y}) p(\theta \mid \mathbf{x}, \mathbf{y}, \mathbf{z}) \, \mathrm{d}\mathbf{z}. \tag{4}$$

Note how this accounts for the unobserved confounders: it assumes that $p(\mathbf{z} \mid \mathbf{x}, \mathbf{y})$ accurately reflects the latent structure. In doing so, we perform inferences for $p(\theta \mid \mathbf{x}, \mathbf{y}, \mathbf{z})$, averaged over posterior samples from $p(\mathbf{z} \mid \mathbf{x}, \mathbf{y})$.

In general, causal inference with latent confounders can be dangerous: it uses the data twice (once to estimate the confounder; another to estimate the mechanism), and thus it may absorb information from each arrow $X_m \to Y$. Why is this justified? We answer this below.

Proposition 1. *Assume the causal graph of Figure 2 (left) is correct and that the true distribution resides in some configuration of the parameters of the causal model. Then the posterior $p(\theta \mid \mathbf{x}, \mathbf{y})$ provides a consistent estimator of the causal mechanism f_y.*

(See Appendix A for the proof.) Proposition 1 rigorizes previous methods in the framework of probabilistic causal models. The intuition is that as more SNPs arrive ("$M \to \infty$, N fixed"), the posterior concentrates at the true confounders z_n, and thus we can estimate the causal mechanism given each data point's confounder z_n. As more data points arrive ("$N \to \infty$, M fixed"), we can estimate the causal mechanism given any confounder z_n as there are infinity of them.

Connecting to Two-Stage Estimation. Existing GWAS methods adjust for latent population structure using two stages (Astle & Balding, 2009): first, estimate the confounders $z_{1:N}$; second, infer the outcome parameters θ given the data set and the estimate of the confounders. To incorporate uncertainty, a Bayesian version would not use a point estimate of $z_{1:N}$ but the full posterior $p(z_{1:N} \mid \mathbf{x}, \mathbf{y})$; then it would infer θ given posterior samples of $z_{1:N}$. Following Equation 4, this is the same as joint posterior inference. Thus the two stage approach is justified as a Bayesian approximation that uses a point estimate of the posterior.

3.2 Implicit Causal Model with a Latent Confounder

Above, we outlined how to specify an implicit causal model for GWAS. We now specify in detail the functions and priors for the confounders z_n, the SNPs x_{nm}, and the traits y_n (Equation 3). Figure 2 (right) visualizes the model we describe below. Appendix B provides an example implementation in the Edward probabilistic programming language (Tran et al., 2016).

Generative Process of Confounders z_n. We use standard normal noise and set the confounder function $g_z(\cdot)$ to the identity. This implies the distribution of confounders $p(z_n)$ is standard normal. Their dimension $z_n \in \mathbb{R}^K$ is a hyperparameter. The dimension K should be set to the highest value such that the latent space most closely approximates the true population structure but smaller than the total number of SNPs to avoid overfitting.

Generative Process of SNPs x_{nm}. To specify the SNPs, we build on an implicit modeling formulation of factor analysis. Factor analysis techniques have been shown to be successful in GWAS applications (Price et al., 2006; Song et al., 2015). In particular, let each SNP be encoded as a 0, 1, or 2 to denote the three possible genotypes. (This is unphased data, where 0 indicates two major alleles; 1 indicates one major and one minor allele; and 2 indicates two minor alleles.) We specify their generative process,

$$\text{logit}\,\pi_{nm} = z_n^\top w_m, \qquad x_{nm} = \mathbb{I}[\epsilon_1 > \pi_{nm}] + \mathbb{I}[\epsilon_2 > \pi_{nm}], \qquad \epsilon_1, \epsilon_2 \sim \text{Uniform}(0, 1).$$

This defines a $\text{Binomial}(2, \pi_{nm})$ distribution on x_{nm}. Analogous to generalized linear models, the Binomial's logit probability is linear with respect to z_n. We then sum up two Bernoulli trials: they are represented as indicator functions of whether a uniform sample is greater than the probability. (The uniform noises are newly drawn for each index n and m.)

Assuming a standard normal prior on the variables w_m, this generative process is equivalent to logistic factor analysis. The variables w_m act as "principal components," embedding the M-many SNPs within a subspace of lower dimension K.

Logistic factor analysis makes strong assumptions: linear dependence on the confounder and that one parameter per dimension has sufficient representational capacity. We relax these assumptions using a neural network over concatenated inputs,

$$\text{logit}\,\pi_{nm} = \text{NN}([z_n, w_m] \,|\, \phi).$$

Similar to the above, the variables w_m serve as principal components. The neural network takes an input of dimension $2K$ and outputs a scalar real value. The neural networks' weights and biases ϕ are shared across the generative process of all SNPs. This enables learning of nonlinear interactions between z_n and w_m. We place a standard normal prior over ϕ.

Generative Process of Traits y_n. To specify the traits, we build on an implicit modeling formulation of linear regression. It is the mainstay tool in GWAS applications (Price et al., 2006; Song et al., 2015). Formally, for real-valued $y \in \mathbb{R}$, we model each observed trait as

$$y_n = [x_{n,1:M}, z_n]^\top \theta + \epsilon_n, \qquad \epsilon_n \sim \text{Normal}(0, 1),$$

This process assumes linear dependence on SNPs, no gene-gene and gene-population interaction, and additive noise. We generalize this model using a neural network over the same inputs,

$$y_n = \text{NN}([x_{n,1:M}, z_n, \epsilon] \,|\, \theta), \qquad \epsilon_n \sim \text{Normal}(0, 1).$$

The neural network takes an input of dimension $M + K + 1$ and outputs a scalar real value; to model categorical outcomes, we discretize the output over equally spaced cutpoints. We place a standard normal prior over the weights and biases θ.

4 Likelihood-Free Variational Inference

We described a rich causal model for how SNPs cause traits and that can adjust for latent population-confounders. Given GWAS data, we aim to infer the posterior of outcome parameters θ (Equation 4). Calculating this posterior reduces to calculating the joint posterior of confounders z_n, SNP parameters w_m and ϕ, and trait parameters θ,

$$p(z_{1:N}, w_{1:M}, \phi, \theta \,|\, \mathbf{x}, \mathbf{y}) \propto p(\phi)p(\theta) \prod_{n=1}^{N} \Big[p(z_n)p(y_n \,|\, x_{n,1:M}, z_n, \theta) \prod_{m=1}^{M} p(w_m)p(x_{nm} \,|\, z_n, w_m, \phi) \Big].$$

This means we can use typical inference algorithms on the joint posterior. We then collapse variables to obtain the marginal posterior of θ. (For Monte Carlo methods, we drop the auxiliary samples; for variational methods, it is given if the variational family follows the posterior's factorization.)

One difficulty is that with implicit models, evaluating the density is intractable: it requires integrating over a nonlinear function with respect to a high-dimensional noise. Thus we require likelihood-free methods, which assume that one can only sample from the model's likelihood (Marin et al., 2012; Tran et al., 2017). Here we apply likelihood-free variational inference (LFVI), which we scale to millions of genetic measurements (Tran et al., 2017).

As with all variational methods, LFVI posits a family of distributions over the latent variables and then optimizes to find the member closest to the posterior. For the variational family, we specify normal distributions with diagonal covariance for the SNP components w_m and confounder z_n,

$$q(w_m) = \text{Normal}(w_m; \mu_{w_m}, \sigma_{w_m} I), \qquad q(z_n) = \text{Normal}(z_n; \mu_{z_n}, \sigma_{z_n} I).$$

We specify a point mass for the variational family on both neural network parameters ϕ and θ. (This is equivalent to point estimation in a variational EM setting.)

For LFVI to scale to massive GWAS data, we use stochastic optimization by subsampling SNPs (Gopalan et al., 2016). At a high level, the algorithm proceeds in two stages. In the first stage, it cycles through the following steps:

1. Sample SNP location m and collect the observations at that location from all individuals.
2. Use the observations and current estimate of the confounders $z_{1:N}$ to update the mth SNP component w_m and SNP neural network parameters ϕ.
3. Use the observations and current estimate of SNP components $w_{1:M}$ to update the confounders $z_{1:N}$.

This first stage infers the posterior distribution of confounders z_n and SNPs parameters w_m and ϕ. Each step's computation is independent of the number of SNPs, allowing us to scale to millions of genetic factors. In experiments, the algorithm converges while scanning over the full set of SNPs only once or twice.

In the second stage, we infer the posterior θ given data and the inferred confounder from the first stage. Appendix C describes the algorithm in more detail; it expands on the LFVI implementation in Edward (Tran et al., 2016).

5 Empirical Study

We described implicit causal models, how to adjust for latent population-based confounders, and how to perform scalable variational inference. In general, validating causal inferences on observational data is not possible (Pearl, 2000). Therefore to validate our work, we perform an extensive simulation study on 100,000 SNPs, 940 to 5,000 individuals, and across 100 replications of 11 settings. The study indicates that our model is significantly more robust to spurious associations, with a state-of-the-art gain of 15-45.3% in accuracy. We also apply our model to a real-world GWAS of Northern Finland Birth Cohorts; our model indeed captures real causal relationships—identifying similar SNPs as previous state of the art.

We compare against three methods that are currently state of the art: PCA with linear regression (Price et al., 2006) ("PCA"); a linear mixed model (with the EMMAX software) (Kang et al., 2010) ("LMM"); and logistic factor analysis with inverse regression (Song et al., 2015) ("GCAT"). In all experiments, we use Adam with a initial step-size of 0.005, initialize neural network parameters uniformly with He variance scaling (He et al., 2015), and specify the neural networks for traits and SNPs as fully connected with two hidden layers, ReLU activation, and batch normalization (hidden layer sizes described below). For the trait model's neural network, we found that including latent variables as input to the final output layer improves information flow in the network.

5.1 Simulation Study: Robustness to Spurious Associations

We analyze 11 simulation configurations, where each configuration uses 100,000 SNPs and 940 to 5,000 individuals. We simulate 100 GWAS data sets per configuration for a grand total of 4,400 fitted models (4 methods of comparison). Each configuration employs a true model to generate the SNPs and traits based on real genomic data. Following Hao et al. (2016), we use the Balding-Nichols model based on the HapMap dataset (Balding & Nichols, 1995; Gibbs et al., 2003); PCA based on

Trait	**ICM**	PCA	LMM	GCAT
HapMap	**99.2**	34.8	30.7	**99.2**
TGP	**85.6**	2.7	43.3	70.3
HGDP	**91.8**	6.8	40.2	72.3
PSD ($a = 1$)	**97.0**	80.4	92.3	95.3
PSD ($a = 0.5$)	**94.3**	79.5	90.1	93.6
PSD ($a = 0.1$)	**92.2**	38.1	38.6	90.4
PSD ($a = 0.01$)	**92.7**	24.2	35.1	90.7
Spatial ($a = 1$)	**90.9**	56.4	60.0	75.2
Spatial ($a = 0.5$)	**86.2**	50.5	46.6	72.5
Spatial ($a = 0.1$)	**80.9**	2.4	26.6	35.6
Spatial ($a = 0.01$)	**75.5**	1.8	15.3	30.2

Table 1: Precision accuracy over an extensive set of configurations and methods; we average over 100 simulations for a grand total of 4,400 fitted models. The setting a in PSD and Spatial determines the amount of sparsity in the latent population structure: lower a means higher sparsity. ICM is significantly more robust to spurious associations, outperforming other methods by up to 45.3%.

Trait	**ICM**	GCAT	LMM	PCA	Uncorrected
Body mass index	0	0	0	0	0
C-reactive protein	2	2	2	2	2
Diastolic blood pressure	0	0	0	0	0
Glucose levels	3	3	2	2	2
HDL cholesterol levels	4	4	4	2	4
Height	1	1	0	0	0
Insulin levels	0	0	0	0	0
LDL cholesterol levels	3	4	3	3	3
Systolic blood pressure	0	0	0	0	0
Triglyceride levels	2	2	3	2	2

Table 2: Number of significant loci at genome-wide significance ($p < 7.2 \times 10^{-8}$) for each of the ten traits from NFBC data. The counts for GCAT are obtained from Song et al. (2015, Table 1); counts for LMM, PCA, and uncorrected are obtained from Kang et al. (2010, Table 2). The implicit causal model (**ICM**) captures causal relationships comparable to previously work.

the 1000 Genomes Project (TGP) (Consortium et al., 2010); PCA based on the Human Genome Diversity project (HGDP) (Rosenberg et al., 2002); four variations of the Pritchard-Stephens-Donelly model (PSD) based on HGDP (Pritchard et al., 2000); and four variations of a configuration where population structure is determined by a latent spatial position of individuals. Only 10 of the 100,000 SNPs are set to be causal. Appendix D provides more detail.

Table 1 displays the precision for predicting causal factors across methods. When failing to account for population structure, "spurious associations" occur between genetic markers and the trait of interest, despite the fact that there is no biological connection. Precision is the fraction of the number of true positives over the number of true and false positives. This measures a method's robustness to spurious associations: higher precision means fewer false positives and thus more robustness.

Table 1 shows that our method achieves state of the art across all configurations. Our method especially dominates in difficult tasks with sparse (small a), spatial (Spatial), and/or mixed membership structure (PSD): there is over a 15% margin in difference to the second best in general, and up to a 45.3% margin on the Spatial ($a = 0.01$) configuration. For simpler configurations, such as a mixture model (HapMap), our method has comparable performance.

5.2 Northern Finland Birth Cohort Data

We analyze a real-world GWAS of Northern Finland Birth Cohorts (Sabatti et al., 2009), which measure several metabolic traits and height and which contain 324,160 SNPs and 5,027 individuals.

We separately fitted 10 implicit causal models, each of which models the effect of SNPs on one of ten traits. To specify the implicit causal models, we set the latent dimension of confounders to be 6 (following Song et al. (2015)). We use 512 units in both hidden layers of the SNP neural network and use 32 and 256 units for the trait neural network's first and second hidden layers respectively. Appendix E provides more detail.

Table 2 compares the number of identified causal SNPs across methods, with an additional "uncorrected" baseline, which does not adjust for any latent population structure. Each method is performed with a subsequent correction as measured by the genomic control inflation factor (Sabatti et al., 2009). Our models identify similar causal SNPs as previous methods. Interestingly, our model tends to agree with Song et al. (2015), identifying a total of 15 significant loci (Song et al. (2015) identified 16; others identified 11-14 loci). This makes sense intuitively, as Song et al. (2015) uses logistic factor analysis which, compared to all methods, most resembles our model.

6 Discussion

We described implicit causal models, a rich class of models that can capture high-dimensional, nonlinear causal relationships. With genome-wide association studies, implicit causal models generalize other models previously shown to be successful and can relax their restrictive assumptions, such as gene-gene interaction, when modeling the trait of interest. In addition, we described an implicit causal model that adjusts for confounders by sharing strength across examples. Our model achieves state-of-the-art accuracy, significantly outperforming existing genetics methods by 15-45.3%.

While we focused on GWAS applications in this paper, we also believe implicit causal models have significant potential in other sciences: for example, to design new dynamical theories in high energy physics; and to accurately model structural equations of discrete choices in economics. We're excited about applications to these new domains, leveraging modern probabilistic modeling and causality to drive new research advances.

References

Babak Alipanahi, Andrew Delong, Matthew T Weirauch, and Brendan J Frey. Predicting the sequence specificities of dna- and rna-binding proteins by deep learning. *Nature Biotechnology*, 33 (8):831–838, 2015.

William Astle and David J Balding. Population structure and cryptic relatedness in genetic association studies. *Statistical Science*, 24(4):451–471, 2009.

David J Balding and Richard A Nichols. A method for quantifying differentiation between populations at multi-allelic loci and its implications for investigating identity and paternity. In *Human identification: The use of DNA markers*, pp. 3–12. 1995.

1000 Genomes Project Consortium et al. A map of human genome variation from population scale sequencing. *Nature*, 467(7319):1061, 2010.

Heather J Cordell. Detecting gene–gene interactions that underlie human diseases. *Nature Reviews Genetics*, 10(6):392–404, 2009.

Robert Culverhouse, Brian K Suarez, Jennifer Lin, and Theodore Reich. A perspective on epistasis: Limits of models displaying no main effect. *The American Journal of Human Genetics*, 70(2): 461–471, 2002.

G Cybenko. Approximation by superpositions of a sigmoidal function. *Mathematics of Control, Signals and Systems*, 2(4):303–314, 1989.

P J Diggle and R J Gratton. Monte Carlo methods of inference for implicit statistical models. *Journal of the Royal Statistical Society Series B*, 1984.

Ronald A Fisher. The correlation between relatives on the supposition of mendelian inheritance. *Philosophical Transactions of the Royal Society of Edinburgh*, 52:399–433, 1918.

Richard A Gibbs, John W Belmont, Paul Hardenbol, Thomas D Willis, FL Yu, HM Yang, Lan-Yang Ch'ang, Wei Huang, Bin Liu, Yan Shen, et al. The international hapmap project. 2003.

P Gopalan, W Hao, D M Blei, and J D Storey. Scaling probabilistic models of genetic variation to millions of humans. *Nature Genetics*, 2016.

W Hao, M Song, and J D Storey. Probabilistic models of genetic variation in structured populations applied to global human studies. *Bioinformatics*, 2016.

Kaiming He, X Zhang, S Ren, and J Sun. Delving deep into rectifiers: Surpassing human-level performance on imagenet classification. In *International Conference on Computer Vision*. IEEE, 2015.

Jennifer L Hill. Bayesian nonparametric modeling for causal inference. *Journal of Computational and Graphical Statistics*, 20(1):217–240, 2011.

Patrik O Hoyer, Dominik Janzing, Joris M Mooij, Jonas Peters, and Prof Bernhard Schölkopf. Nonlinear causal discovery with additive noise models. In *Neural Information Processing Systems*, 2009.

Guido Imbens and Donald B Rubin. *Causal Inference*. Cambridge University Press, 2015.

Fredrik D Johansson, Uri Shalit, and David Sontag. Learning representations for counterfactual inference. In *International Conference on Machine Learning*, 2016.

Hyun Min Kang, Jae Hoon Sul, Susan K Service, Noah A Zaitlen, Sit-yee Kong, Nelson B Freimer, Chiara Sabatti, and Eleazar Eskin. Variance component model to account for sample structure in genome-wide association studies. *Nature Genetics*, 42(4):348–354, 2010.

Christos Louizos, Uri Shalit, Joris Mooij, David Sontag, Richard Zemel, and Max Welling. Causal effect inference with deep latent-variable models. 2017.

Jean-Michel Marin, Pierre Pudlo, Christian P Robert, and Robin J Ryder. Approximate bayesian computational methods. *Statistics and Computing*, 22(6):1167–1180, 2012.

Brett A McKinney, David M Reif, Marylyn D Ritchie, and Jason H Moore. Machine learning for detecting gene-gene interactions. *Applied Bioinformatics*, 5(2):77–88, 2006.

Joris M Mooij, Oliver Stegle, Dominik Janzing, Kun Zhang, and Bernhard Schoelkopf. Probabilistic latent variable models for distinguishing between cause and effect. In *Neural Information Processing Systems*, 2010.

Kevin P Murphy. *Machine Learning: A Probabilistic Perspective*. MIT press, 2012.

J Pearl. *Causality*. Cambridge University Press, 2000.

Judea Pearl. *Probabilistic reasoning in intelligent systems: networks of plausible inference*. Morgan Kaufmann, 1988.

Alkes L Price, Nick J Patterson, Robert M Plenge, Michael E Weinblatt, Nancy A Shadick, and David Reich. Principal components analysis corrects for stratification in genome-wide association studies. *Nature Genetics*, 38(8):904–909, 2006.

Jonathan K Pritchard, Matthew Stephens, and Peter Donnelly. Inference of population structure using multilocus genotype data. *Genetics*, 155(2):945–959, 2000.

Danilo J Rezende, Shakir Mohamed, and Daan Wierstra. Stochastic backpropagation and approximate inference in deep generative models. In *International Conference on Machine Learning*, 2014.

Noah A Rosenberg, Jonathan K Pritchard, James L Weber, Howard M Cann, Kenneth K Kidd, Lev A Zhivotovsky, and Marcus W Feldman. Genetic structure of human populations. *Science*, 298(5602):2381–2385, 2002.

Chiara Sabatti, Susan K Service, Anna-Liisa Hartikainen, Anneli Pouta, Samuli Ripatti, Jae Brodsky, Chris G Jones, Noah A Zaitlen, Teppo Varilo, Marika Kaakinen, et al. Genome-wide association analysis of metabolic traits in a birth cohort from a founder population. *Nature genetics*, 41 (1):35–46, 2009.

Minsun Song, Wei Hao, and John D Storey. Testing for genetic associations in arbitrarily structured populations. *Nature*, 47(5):550–554, 2015.

Peter Spirtes, Clark Glymour, and Richard Scheines. *Causation, prediction, and search*. Springer-Verlag, 1993.

Dustin Tran, Alp Kucukelbir, Adji B Dieng, Maja Rudolph, Dawen Liang, and David M Blei. Edward: A library for probabilistic modeling, inference, and criticism. *arXiv preprint arXiv:1610.09787*, 2016.

Dustin Tran, Rajesh Ranganath, and David M Blei. Deep and hierarchical implicit models. In *Neural Information Processing Systems*, 2017.

Stefan Wager and Susan Athey. Estimation and inference of heterogeneous treatment effects using random forests. *arXiv preprint arXiv:1510.04342*, 2015.

Bruce S Weir and C Clark Cockerham. Estimating f-statistics for the analysis of population structure. *Evolution*, 38(6):1358–1370, 1984.

Jianming Yu, Gael Pressoir, William H Briggs, Irie Vroh Bi, Masanori Yamasaki, John F Doebley, Michael D McMullen, Brandon S Gaut, Dahlia M Nielsen, James B Holland, Stephen Kresovich, and Edward S Buckler. A unified mixed-model method for association mapping that accounts for multiple levels of relatedness. *Nature Genetics*, 38(2):203–208, 2005.

Kun Zhang and Aapo Hyvärinen. On the identifiability of the post-nonlinear causal model. In *Uncertainty in Artificial Intelligence*, pp. 647–655, 2009.

A CONSISTENCY

Consider the simplest setting in § 2, where the causal graph is as shown with a global confounder with finite dimension and where we observe set $\{(x_n, y_n)\}$. Assume the specified model family over the causal graph includes the true data generating process.

First consider consider an atomic intevention $\mathrm{do}(X = x)$ and let β^* be the true structural value that generated our observations. The probability of a new outcome given the intervention and global structure is

$$p^*(y \mid \mathrm{do}(X = x), \beta^*)) = p^*(y \mid x, \beta^*).$$

This follows from the backdoor criterion on the empty set. By Bernstein von-Mises, the posterior for our model $p(\beta \mid \mathbf{x}, \mathbf{y})$ concentrates at β^*. Thus, similarly, our posterior for θ given β^* concentrates to the true functional mechanism f_y. This implies we have a consistent estimate of $p^*(y \mid \mathrm{do}(\cdot), \beta^*)$.

This simple proof rigorizes the ideas behind learning and fixing population structure, a common heuristic in GWAS methods. Moreover, it lets us understand how uncertainty estimates of the latent structure become important as we apply these methods to finite data in practice.

B IMPLICIT CAUSAL MODEL IN EDWARD

We provide an example of an implicit causal model written in the Edward language below.

```
import edward as ed
import tensorflow as tf

M = 100000  # number of SNPs
N = 5000  # number of individuals
K = 25  # latent dimension

def snp_neural_network(z, w):
  z_tile = tf.tile(tf.reshape(z, [N, 1, K]), [1, M, 1])
  w_tile = tf.tile(tf.reshape(w, [1, M, K]), [N, 1, 1])
  h = tf.concat([z_tile, w_tile], 1),
  h = tf.layers.dense(h, 32, activation=tf.nn.relu)
  h = tf.layers.dense(h, 256, activation=tf.nn.relu)
  h = tf.layers.dense(h, 1, activation=None)
  return tf.reshape(h, [N, M])

def trait_neural_network(z, x):
  h = tf.layers.dense(tf.concat([z, x], 1), 10, activation=tf.nn.relu)
  h = tf.layers.dense(h, 10, activation=tf.nn.relu)
  h = tf.concat([z, h], 1)  # include connection to z for output layer
  h = tf.layers.dense(h, 1, activation=None)
  return tf.reshape(h, [N])

z = Normal(loc=0.0, scale=1.0, sample_shape=[N, K])
w = Normal(loc=0.0, scale=1.0, sample_shape=[M, K])
logits = snp_neural_network(z, w)
x = Binomial(total_count=2.0, logits=logits)

# Note: Sometimes it's preferable to have neural net parameterize a
# distribution for tractable density, e.g., if trait is discrete.
y = trait_neural_network(z, x)
```

C LIKELIHOOD-FREE VARIATIONAL INFERENCE FOR GWAS

C.1 VARIATIONAL OBJECTIVE

The log-likelihood per-individual and per-SNP is

$$\log p(x_{nm}, y_n \mid w_m, z_n, \theta, \phi) = \log p(y_n \mid x_{n,1:M}, z_n, \theta) + \log p(x_{nm} \mid w_m, z_n, \phi).$$

There are local priors $p(w_m)$, $p(z_n)$ and global priors $p(\theta)$, $p(\phi)$. The posterior factorizes as

$$p(z_{1:N}, w_{1:M}, \phi, \theta \mid \mathbf{x}, \mathbf{y})$$
$$= p(\phi \mid \mathbf{x}) p(\theta \mid \mathbf{x}, \mathbf{y}) \prod_{m=1}^{M} p(w_m \mid x_{1:N,M}, \phi) \prod_{n=1}^{N} p(z_n \mid x_{n,1:M}, y_n, \theta, \phi, w_{1:M}).$$

Let the variational family follow the posterior's factorization above. For notational convenience, we drop the data dependence in q, $q(\phi) = q(\phi \mid \mathbf{x})$, $q(\theta) = q(\theta \mid \mathbf{x}, \mathbf{y})$ $q(w_m \mid \phi) = q(w_m \mid x_{1:N,m}, \phi)$, $q(z_n \mid \theta, \phi, w_{1:M}) = q(z_n \mid x_{n,1:M}, y_n, \theta, \phi, w_{1:M})$. We write the evidence lower bound and decompose the model's log joint density and the variational density,

$$\begin{aligned}
\mathcal{L} = & \sum_{m=1}^{M} \sum_{n=1}^{N} \mathbb{E}_{q(\phi)q(w_m \mid \phi)q(\theta)q(z_n \mid \theta, \phi, w_{1:M})} \Big[\log p(x_{nm} \mid w_m, z_n, \phi) \Big] + \\
& \sum_{n=1}^{N} \mathbb{E}_{q(\phi)q(w_{1:M} \mid \phi)q(\theta)q(z_n \mid \theta, \phi, w_{1:M})} \Big[\log p(y_n \mid x_{n,1:M}, z_n, \theta) \Big] + \\
& \sum_{m=1}^{M} \mathbb{E}_{q(\phi)q(w_m \mid \phi)} \Big[\log p(w_m) - \log q(w_m \mid \phi) \Big] + \\
& \sum_{n=1}^{N} \mathbb{E}_{q(\phi)q(w_{1:M} \mid \phi)q(\theta)q(z_n \mid \theta, \phi, w_{1:M})} \Big[\log p(z_n) - \log q(z_n \mid \theta, \phi, w_{1:M}) \Big] + \\
& \mathbb{E}_{q(\phi)}[\log p(\phi) - \log q(\phi)] + \mathbb{E}_{q(\theta)}[\log p(\theta) - \log q(\theta)].
\end{aligned}$$

Assume that the variational family for z_n and w_m are independent of other variables, $q(z_n)$ and $q(w_m)$. Also assume delta point masses for $q(\theta) = \mathbb{I}[\theta - \theta']$ parameterized by θ' and $q(\phi) = \mathbb{I}[\phi - \phi']$ parameterized by ϕ'. This simplifies the objective, reducing to

$$\begin{aligned}
\mathcal{L} = & \sum_{m=1}^{M} \sum_{n=1}^{N} \mathbb{E}_{q(w_m)q(z_n)} \Big[\log p(x_{nm} \mid w_m, z_n, \phi') \Big] + \sum_{n=1}^{N} \mathbb{E}_{q(z_n)} \Big[\log p(y_n \mid x_{n,1:M}, z_n, \theta') \Big] + \\
& \sum_{m=1}^{M} \mathbb{E}_{q(w_m)} \Big[\log p(w_m) - \log q(w_m) \Big] + \sum_{n=1}^{N} \mathbb{E}_{q(z_n)} \Big[\log p(z_n) - \log q(z_n) \Big] + \\
& \log p(\phi') + \log p(\theta').
\end{aligned}$$

Each expectation can be unbiasedly estimated with Monte Carlo. For gradient-based optimization, we use reparameterization gradients (Rezende et al., 2014), which we detail in the next subsection.

C.2 First Stage: Learning the Confounder

We provide details for the gradients. Let λ_{w_m} parameterize $q(w_m; \lambda_{w_m})$ and λ_{z_n} parameterize $q(z_n; \lambda_{z_n})$. We are interested in training the parameters $\lambda_{w_m}, \lambda_{z_n}, \theta', \phi'$. Subsample a SNP location $m \in \{1, \dots, M\}$. Draw a sample $z'_n \sim q(z_n; \lambda_{z_n})$ for $n = 1, \dots, N$ and $w'_m \sim q(w_m; \lambda_{w_m})$ for $m = 1, \dots, M$, where the samples are reparameterizable (see Rezende et al. (2014) for details).

The gradient with respect to parameters λ_{z_n} is unbiasedly estimated by

$$\nabla_{\lambda_{z_n}} \mathcal{L} \approx \nabla_{\lambda_{z_n}} \Big[\log p(x_{nm} \mid w'_m, z'_n, \phi') + \log p(y_n \mid x_{n,1:M}, z'_n, \theta') + \log p(z'_n) - \log q(z'_n) \Big].$$

This gradient scales linearly with the number of SNPs M. This is undesirable as the number of SNPs ranges from the hundreds of thousands to millions. We prevent this scaling by observing that for large M, the information in $x_{n,1:M}$ will influence the posterior far more than the single scalar y_n. In math, $p(z_n \mid x_{n,1:M}, y_n, \theta, \phi, w_{1:M}) \approx p(z_n \mid x_{n,1:M}, \theta, \phi, w_{1:M})$. This is a tacit assumption in all GWAS methods that adjust for the confounder (Yu et al., 2005; Price et al., 2006; Astle & Balding, 2009; Kang et al., 2010).

The gradient with respect to parameters λ_{z_n} simplifies to

$$\nabla_{\lambda_{z_n}} \mathcal{L} \approx \nabla_{\lambda_{z_n}} \Big[\log p(x_{nm} \,|\, w'_m, z'_n, \phi') + \log p(z'_n) - \log q(z'_n) \Big],$$

which scales to massive numbers of SNPs.

The gradients with respect to parameters λ_{w_m} and ϕ' are unbiasedly estimated by

$$\nabla_{\lambda_{w_m}} \mathcal{L} \approx \sum_{n=1}^{N} \Big[\nabla_{\lambda_{w_m}} \log p(x_{nm} \,|\, w'_m, z'_n, \phi') \Big] + \nabla_{\lambda_{w_m}} \log p(w'_m) - \nabla_{\lambda_{w_m}} \log q(w'_m),$$

$$\nabla_{\phi'} \mathcal{L} \approx \sum_{n=1}^{N} \nabla_{\phi'} \log p(x_{nm} \,|\, w'_m, z'_n, \phi').$$

Note how none of this depends on the trait y or trait parameters θ. We can thus perform inference to first approximate the posterior $p(z_{1:N}, w_{1:M}, \phi \,|\, \mathbf{x}, \mathbf{y})$. In a second stage, we can then perform inference to approximate the posterior $p(\theta \,|\, z_{1:N}, w_{1:M}, \mathbf{x}, \mathbf{y})$. The computational savings is significant not only within task but across tasks: when modelling many traits of interest (for example, § 5.2). inference over the SNP confounders only needs to be done once and can be re-used. We perform stochastic gradient ascent using these gradients to maximize the variational objective.

C.3 Second Stage: Learning the Trait

Above we described the first stage of an algorithm which performs stochastic gradient ascent to optimize parameters so that $q(z_n)q(w_{1:M})q(\theta') \approx p(z_{1:N}, w_{1:M}, \phi \,|\, \mathbf{x}, \mathbf{y})$. Given these optimized parameters, we are interested in training θ'. Dropping constants with respect to θ in the objective, we have

$$\mathcal{L} \propto \sum_{n=1}^{N} \mathbb{E}_{q(z_n)} \Big[\log p(y_n \,|\, x_{n,1:M}, z_n, \theta') \Big] + \log p(\theta').$$

We maximize this objective using stochastic gradients with a single Monte Carlo sample, $z'_n \sim q(z_n)$,

$$\nabla_{\theta'} \mathcal{L} \approx \sum_{n=1}^{N} \nabla_{\theta'} \log p(y_n \,|\, x_{n,1:M}, z'_n, \theta') + \nabla_{\theta'} \log p(\theta')$$

This corresponds to Monte Carlo EM. Its primary computation per-iteration is the backward pass of the neural network.

D Simulation Study

We provide more detail to § 5.1. Implicit causal models can not only represent many causal structures but, more importantly, learn them from data. To demonstrate this, we simulate data from a comprehensive collection of popular models in GWAS and analyze how well the fitted model can capture them. These configurations exactly follow Hao et al. (2016) with same hyperparameters, which we describe below.

For each of the 11 simulation configurations, we generate 100 independent data sets. Each data set consists of a $M \times N$ matrix of genotypes X and vector of N traits y. Each individual n has M SNPs and one trait.

D.1 Genotype Matrix

To simulate the $M \times N$ matrix of genotypes X, we draw $x_{mn} \sim \text{Binomial}(2, \pi_{mn})$ for $m = 1, \ldots, M$ SNPs and $n = 1, \ldots, N$ individuals. The probabilities π_{mn} can be encoded under a real-valued $M \times N$ matrix of allele frequencies F where $\pi_{mn} = [\text{logit}(F)]_{mn}$.

Many models in GWAS can be described under the factorization $F = \Gamma S$, where Γ is a $M \times K$ matrix and S is a $K \times N$ matrix for a fixed rank $K \leq N$. This includes principal components analysis (Price

et al., 2006), the Balding-Nichols model (Balding & Nichols, 1995), and the Pritchard-Stephens-Donnelly model (Pritchard et al., 2000). The $M \times K$ matrix Γ describes how structure manifests in the allele frequencies across SNPs. The $K \times N$ matrix S encapsulates the genetic population structure across individuals.

We describe how we form Γ and S for each of the 11 simulation configurations.

Balding-Nichols Model (BN) + HapMap. The BN model describes individuals according to a discrete mixture of ancestral subpopulations (Balding & Nichols, 1995). The HapMap data set was collected from three discrete populations (Gibbs et al., 2003), which allows us to populate each row m of Γ with three i.i.d. draws from the Balding-Nichols model: $\Gamma_{mk} \sim \mathrm{BN}(p_m, F_m)$, where $k \in \{1, 2, 3\}$. Each Γ_{mk} is interpreted to be the allele frequency for subpopulation k at SNP m. The pairs (p_m, F_m) are computed by randomly selecting a SNP in the HapMap data set, calculating its observed allele frequency, and estimating its F_{ST} value using the estimator of Weir & Cockerham (1984). The columns of S are populated with indicator vectors such that each individual is assigned to one of the three subpopulations. The subpopulation assignments are drawn independently with probabilities $60/210$, $60/210$, and $90/210$, which reflect the subpopulation proportions in the HapMap data set. The simulated data has $M = 100,000$ SNPs and $N = 5000$ individuals.

1000 Genomes Project (TGP). TGP is a project that comprehensively catalogs human genetic variation by producing complete genome sequences of well over 1000 individuals of diverse ancestries (Consortium et al., 2010). To form Γ, we sample $\Gamma_{mk} \sim 0.9\,\mathrm{Uniform}(0, 1/2)$ for $k = 1, 2$ and set $\Gamma_{m3} = 0.05$. To form S, we compute the first two principal components of the TGP genotype matrix after mean centering each SNP. We then transform each principal component to be between $(0, 1)$ and set the first two rows of S to be the transformed principal components. The third row of S is set to 1 as an intercept. The simulated data has $M = 100,000$ SNPs and $N = 1500$ individuals (the total number of individuals in the TGP data set).

Human Genome Diversity Project (HGDP). HGDP is an international project that has genotyped a large collection of DNA samples from individuals distributed around the world, aiming to assess worldwide genetic diversity at the genomic level (Rosenberg et al., 2002). We followed the same scheme as for TGP above. The simulated data has $M = 100,000$ SNPs and $N = 940$ individuals (the total number of individuals in the HGDP data set).

Pritchard-Stephens-Donnelly (PSD) + HGDP. The PSD model describes individuals according to an admixture of ancestral subpopulations (Pritchard et al., 2000). The rows of Γ are drawn from three i.i.d. draws from the Balding-Nichols model: $\Gamma_{mk} \sim \mathrm{BN}(p_m, F_m)$, where $k \in \{1, 2, 3\}$. The pairs (p_m, F_m) are computed by randomly selecting a SNP in the HGDP data set, calculating its observed allele frequency, and estimating its F_{ST} value using the estimator of Weir & Cockerham (1984). The estimator requires each individual to be assigned to a subpopulation, which are made according to the $K = 5$ subpopulations from the analysis in Rosenberg et al. (2002). The columns of S are sampled $(s_{1n}, s_{2n}, s_{3n}) \sim \mathrm{Dirichlet}(\boldsymbol{\alpha} = (a, a, a))$ for $n = 1, \ldots, N$. We apply four PSD configurations with hyperparameter settings of $a = 0.01, 0.1, 0.5, 1$. Varying a from 1 to 0 varies the level of sparsity as individuals are placed from uniformly to corners of the simplex. The simulated data has $M = 100,000$ SNPs and $N = 5000$ individuals.

Spatial. In this setting, we simulate genotypes such that the population structure relates to the spatial position of individuals. The matrix Γ is populated by sampling $\Gamma_{mk} \sim 0.9\,\mathrm{Uniform}(0, 1/2)$ for $k = 1, 2$ and setting $\Gamma_{m3} = 0.05$. The first two rows of S correspond to coordinates for each individual on the unit square and are set to be independent and identically distributed samples from $\mathrm{Beta}(a, a)$, while the third row of S is set to 1 as an intercept. We apply four spatial configurations with hyperparameter settings of $a = 0.01, 0.1, 0.5, 1$. As with the Dirichlet distribution in the PSD model, varying a from 1 to 0 varies the level of sparsity as individuals are placed from uniformly to corners of the unit square. The simulated data has $M = 100,000$ SNPs and $N = 5000$ individuals.

D.2 Traits of Interest

To simulate traits y, we simulate from a linear model: for each individual n's SNPs $\{x_{mn}\}$,

$$y_n = \sum_{m=1}^{M} \beta_m x_{mn} + \lambda_n + \epsilon_n, \qquad \epsilon_n \sim \mathrm{Normal}(0, \sigma_n^2).$$

Each trait is real-valued and is determined by a linear combination of SNPs, a per-individual offset, and heteroskedastic noise. Below we describe how we set $\{\beta_m\}$, $\{\lambda_n\}$, and $\{\sigma_n\}$.

Without loss of generality, we set the first 10 SNPs to be true alternative SNPs ($\beta_m \neq 0$), where $\beta_m \sim \text{Normal}(0, 0.5)$ for $m = 1, 2, \ldots, 10$; $\beta_m = 0$ for $m > 10$. In order to simulate λ_j and ϵ_j so that they are also influenced by the latent variables $z_1, \ldots, z_n$, we performed the following:

1. Run K-means clustering on the columns of S with $K = 3$ using Euclidean distance. This assigns each individual j to one of three partitions S_1, S_2, S_3 where $S_k \subset 1, 2, \ldots, n$.
2. Set $\lambda_j = k$ for all $j \in S_k$ for each $k = 1, 2, 3$.
3. Draw $\tau_1^2, \tau_2^2, \tau_3^2 \sim \text{InverseGamma}(3, 1)$. Set $\sigma_j = \tau_k$ for all $j \in S_k$.

Following Song et al. (2015),

> This strategy simulates non-genetic effects and random variation that manifest among K discrete groups over a more continuous population genetic structure defined by S. This is meant to emulate the fact that environment (specifically lifestyle) may partition among individuals in a manner distinct from, but highly related to population structure.

We apply this strategy for each of the 11 configurations where each involved up to $M = 100,000$ SNPs and $N = 5000$ individuals. For each configuration, we simulated 100 independent data sets, thus requiring a total of 1100 fitted models per method of comparison.

D.3 Other Details

After fitting each model, we obtain one p-value for each SNP, which is the probability that the SNP's effect on the trait of interest is zero. We fix a p-value threshold of $t = 0.0025$. To calculate the number of observed positives, we count the number of p-values for that are less than or equal to t. The true positives are the subset of p-values associated with causal SNPs; false positives are those associated with null SNPs.

Spurious associations occur when p-values corresponding to null SNPs are artificially small. Namely, false positives are spurious associations. In general, we expect there to be $m_0 \times t$ false positives among the m_0 p-values corresponding to null SNPs; in our setting, this corresponds to $(100,000 - 10) \cdot 0.0025 \approx 250$ SNPs. A method properly accounts for structure when the average excess is no more than this number.

To specify the implicit causal model in our experiments, we set the latent dimension of confounders equal to 3 or 5. We use 512 units in both hidden layers of the SNP neural network and use 32 and 256 units for the trait neural network's first and second hidden layers respectively.

E Northern Finland Birth Cohort Data

We provide more detail to § 5.2. The data was obtained from the database of Genotypes and Phenotypes (dbGaP) (`phs000276.v1.p1`). We follow the same preprocessing as Song et al. (2015),

> Individuals were filtered for completeness (maximum 1% missing genotypes) and pregnancy. (Pregnant women were excluded because we did not receive IRB approval for these individuals.) SNPs were first filtered for completeness (maximum 5% missing genotypes) and minor allele frequency (minimum 1% minor allele frequency), then tested for Hardy-Weinberg equilibrium (p-value < $1/328348$). The final dimensions of the genotype matrix are $m = 324,160$ SNPs and $n = 5027$ individuals.
>
> A Box-Cox transform was applied to each trait, where the parameter was chosen such that the values in the median 95% value of the trait was as close to the normal distribution as possible. Indicators for sex, oral contraception, and fasting status were added as adjustment variables. For glucose, the individual with the minimum value was removed from the analysis as an extreme outlier.

No additional changes were made to the data.

After fitting each model, we follow the same procedure as in the simulation study for predicting causal factors. We set the p-value threshold to be the genome-wide threshold of 7.2×10^{-8} following Kang et al. (2010).